Nanoscale diffusion in amorphous $Fe_{75}Zr_{25}$ films

Ajay Gupta,[1,*] Sujoy Chakravarty,[1,†] A. K. Tyagi,[2] and Rudolf Rüffer[3]
[1]*UGC-DAE Consortium for Scientific Research, University Campus, Khandwa Road, Indore 452017, India*
[2]*Materials Science Division, Indira Gandhi Center for Atomic Research, Kalpakkam 603102, India*
[3]*European Synchrotron Radiation Facility, BP 220, F-38043 Grenoble Cedex, France*
(Received 17 April 2008; published 18 December 2008)

Self-diffusion of Fe in amorphous $Fe_{75}Zr_5$ films has been studied over a wide temperature range by combining secondary-ion-mass spectrometry and nuclear-resonance reflectivity measurements. Subnanometer accuracy of nuclear-resonance reflectivity in diffusion length measurement allows quantitative determination of time-dependent diffusivity of Fe during structural relaxation. A clear correlation between diffusivity and different types of structural relaxations is observed. It is found that in both structurally relaxed and unrelaxed states, diffusive jumps occur via a collective motion of a group of atoms. However, the presence of excess free volume in unrelaxed amorphous films causes the activation energy as well as the diffusion entropy to decrease, suggesting that the average number of atoms participating in a diffusive jump is significantly less as compared to that in the fully relaxed state. The typical diffusion length involved in annihilation of free volume is 0.7 nm, which agrees with the length scale of structural fluctuations as seen in neutron- and x-ray-scattering experiments.

DOI: 10.1103/PhysRevB.78.214207 PACS number(s): 66.30.Fq, 64.70.pe, 76.80.+y

I. INTRODUCTION

Thin films of amorphous alloys have attracted a great deal of attention in recent years, as they possess several advantages over polycrystalline films in terms of various physical properties such as magnetic, mechanical, and electrical properties.[1–5] Due to the absence of grains and grain boundaries, amorphous films generally have low surface roughness and thus present sharper interfaces in multilayer structures. As a result, they find increasing applications in spin valve and tunnel magnetoresistance devices.[1,2] Because of the absence of long-range order, they possess isotropic properties and are potential candidates for future applications in micro-sized mechanical devices.[3] The absence of grain boundaries also makes them useful as diffusion barriers in microchip fabrication.[4,5] However, the amorphous phase is metastable in nature and thermal annealing may cause structural relaxation and/or its transformation to stable crystalline phases, resulting in drastic changes in almost all of its physical properties. Since such structural transformations are governed by atomic diffusion of the constituent species, self-diffusion in amorphous alloys has been a subject of vital importance and has been studied extensively.[6–10] However, most of the studies in the literature pertain to the structurally relaxed amorphous state. It may be noted that in conventional applications of amorphous alloy ribbons, generally, a fully relaxed state is used, so as to avoid any variation in the properties with time. On the other hand, applications of amorphous thin films pertain to unrelaxed or partially relaxed state only. This is because of the fact that the thermal annealing required to achieve a fully relaxed structure may obscure the interfaces in a multilayer due to excessive interdiffusion at the interfaces, resulting in deterioration of their properties. Therefore, in view of the recent applications of amorphous thin films, it is important to understand the atomic diffusion in unrelaxed or partially relaxed amorphous state. Though, over the last few years, the knowledge of the diffusion mechanism in the relaxed amorphous state has increased considerably, there are still open questions on the diffusion behavior during structural relaxation.

As-deposited films may contain a large density of structural defects in terms of excess quenched-in free volume, internal stresses, etc. Subsequent thermal annealing is known to produce structural relaxation in the system, as it tries to minimize the internal energy and evolves toward the local thermal equilibrium structure. Such structural relaxation results in significant changes in almost all physical properties of amorphous alloys, and therefore has been studied extensively in the literature.[11–17] Generally, structural relaxation is studied by monitoring one of the physical properties such as mass density, electrical resistivity, or magnetic properties as a function of annealing temperature and time.[13–15] Microstructural changes as observed using diffraction,[16,17] or spectroscopic techniques,[18] have also been studied in order to understand the structural relaxation in amorphous alloys. It may be noted that structural relaxation is primarily governed by atomic diffusion of the constituent species. However, very few studies exist in the literature on the variation in atomic diffusivity with structural relaxation. Although it was realized rather early that structural relaxation affects significantly the atomic diffusion and vice versa in amorphous alloys,[19] very few systematic studies exist on the effect of structural relaxation on atomic diffusion. One of the difficulties in the study of the effect of structural relaxation on atomic diffusion is the small diffusion lengths involved during structural relaxation, which lie in the range of a few nanometers to a fraction of a nanometer. On the other hand, typical depth resolution of conventional depth-profiling techniques such as secondary-ion-mass spectrometry (SIMS) or radioactive tracer technique is on the order of a few nanometers. Thus, for studying the effect of structural relaxation on atomic diffusion, experimental techniques are needed which are capable of measuring diffusion lengths down to a fraction of a nanometer.

Measurements of diffusion lengths in subnanometer range is also important in the case of multilayer structures where even a small interdiffusion at the interfaces can drastically affect their physical properties.[20–22] Since the typical thickness of interfacial regions in multilayer nanostructures is on the order of a nanometer, it is necessary to measure diffusion lengths with subnanometer accuracy, in order to understand the role of interfaces in determining the properties of the multilayer.

Nuclear-resonance reflectivity (NRR) from compositionally homogeneous isotopic multilayers introduced in Ref. 23 is a technique capable of measuring self-diffusion of the constituent species with subnanometer resolution. In the present work we have studied the inter-relation between structural relaxation and self-diffusion of iron in an amorphous Fe-Zr alloy using NRR. The diffusivity at higher temperatures is studied using SIMS. The two techniques combined together provide self-diffusivity of iron in the system over a wide temperature range. While SIMS measurements provide information about diffusivity in structurally relaxed state, NRR measurements are used to follow the evolution of diffusivity with structural relaxation in the system.

II. EXPERIMENTAL DETAILS

Thin films of amorphous Fe-Zr alloy were prepared by ion-beam sputtering of a composite target of Fe and Zr with an Ar (99.9995% purity) ion beam of 800 eV energy and a beam current of 25 mA.[24] The ion gun used was a 3 cm broad-beam Kaufman-type hot-cathode gun (Commonwealth Scientific Corporation). With a base pressure of 1×10^{-7} mbar, the Ar gas flow in the chamber was controlled using a mass flow controller (MKS-MFC 1179A) at 5.0 SCCM (standard cubic centimeters per minute at STP). Initially the chamber was flushed repeatedly with argon gas to remove contamination of other gases. The ion beam was incident at the target at an angle of 45°, and the substrate was kept at a distance of about 20 cm in a direction parallel to the target. Small pieces of zirconium (99.95% purity) were fixed on the iron target. The area covered by the Zr target was controlled in order to achieve the desired composition of the deposited alloy. Two different targets, one with natural Fe (99.99% purity) and the other one enriched in ^{57}Fe (better than 99.99% elemental purity), were used in order to deposit layers with different isotopic abundances of iron. Two sets of samples, one with an isotopic multilayer structure and the other with an isotopic marker layer, were prepared. The nominal structure of the isotopic multilayer sample was float glass substrate/$[^{57}Fe_{75}Zr_{25}(3\ nm)/Fe_{75}Zr_{25}(4\ nm)] \times 10$, while that of the marker layer sample was float glass substrate/$Fe_{75}Zr_{25}(30\ nm)/^{57}Fe_{75}Zr_{25}(4\ nm)/Fe_{75}Zr_{25}(30\ nm)$. Both the isotopic marker layer and multilayer samples of amorphous $Fe_{75}Zr_{25}$ were prepared in the same run and under identical conditions so that both the samples are chemically homogeneous and have the same chemical composition. The multilayer was used to study self-diffusion of iron at lower temperatures using NRR, while the marker layer was used for studies at comparatively higher temperatures using SIMS.

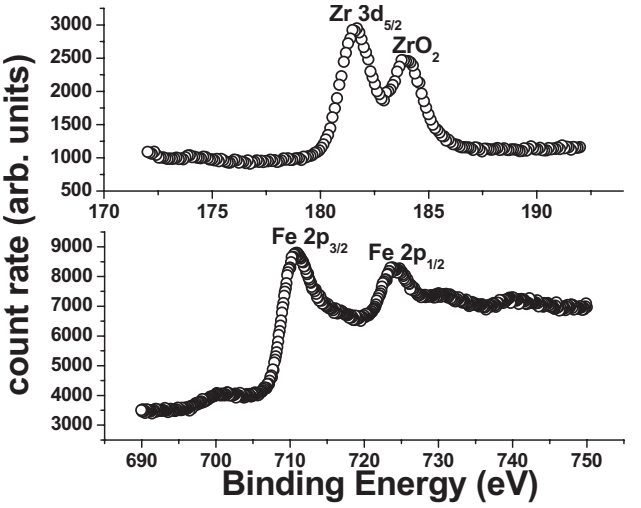

FIG. 1. XPS spectra of FeZr film covering the binding-energy ranges corresponding to Zr $3d_{5/2}$ and Fe $2p_{3/2}$ levels.

Structural characterization of the samples was carried out with x-ray reflectivity (XRR) and grazing incidence x-ray diffraction (GIXRD) using a Bruker D8 x-ray diffractometer with Cu $K\alpha$ radiation. The composition of the film was obtained from x-ray photoemission spectroscopy (XPS). The XPS data were collected using 1486.6 eV Al $K\alpha$ radiation. The base pressure in the chamber during the measurement was better than 2×10^{-9} mbar. Before recording the XPS patterns, the sample was sputtered with 4 keV Ar^+ ions for 120 min with a small ion current of 10–15 μA in order to remove the surface contamination without changing the composition of the sample. The annealing of the samples for diffusion measurements was performed in a vacuum furnace with a vacuum better than 10^{-6} mbar. The temperature in the furnace was controlled with an accuracy of ± 1 K.

For diffusion measurements, the concentration profile as a function of depth was measured using a CAMECA IMS5F secondary-ion-mass spectrometer. The primary ions used for sputtering were Cs^+ ions of energy 4 keV and the ion current was 30 nA. The secondary ions were detected by a double-focusing magnetic mass spectrometer.

Nuclear-resonance reflectivity of the multilayer samples was measured at the beamline ID18 of European Synchrotron Radiation Facility, Grenoble.[25] The storage ring operated in 16-bunch mode, providing short pulses of x rays every 176 ns. The radiation from the undulator source, optimized for the 14.4 keV transition in iron, was filtered by a double Si (111) reflection followed by a high-resolution nested monochromator. The delayed events, resulting from the nuclear-resonance reflectivity, were separated from the prompt events using a fast avalanche photodiode detector and the associated electronics with a time resolution of 1 ns. While the prompt events (0–5 ns) gave the usual electronic reflectivity, the delayed events (10–160 ns) were used to obtain the nuclear-resonance reflectivity.

III. RESULTS

A. Microstructural studies and thermal stability

Figure 1 shows the XPS of the FeZr sample. The spec-

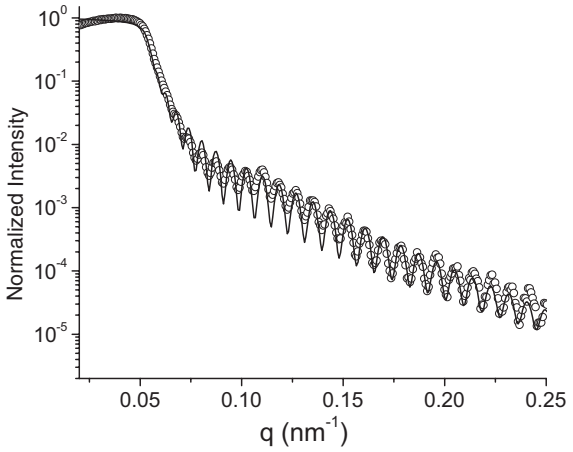

FIG. 2. X-ray reflectivity of the as-deposited amorphous $Fe_{75}Zr_{25}$ isotopic multilayer sample taken using Cu $K\alpha$ radiation.

trum shows the peaks at binding energies corresponding to the core levels of Fe $2p_{3/2}$, Fe $2p_{1/2}$, and Zr $3d_{5/2}$. Apart from these, an additional peak is at binding energy corresponding to ZrO_2. The stoichiometry of the film as obtained from the XPS data is $Fe_{75}Zr_{25}$. A small amount of oxygen was also detected which may be due to an incomplete removal of surface contamination.

Figures 2 and 3 show the x-ray reflectivity patterns of the isotopic multilayer and the marker layer samples, respectively. Both the reflectivity patterns exhibit only the Kiessig oscillations due to the total thickness of the film. The absence of any Bragg peak corresponding to the bilayer periodicity in Fig. 2 suggests that the chemical compositions of the isotopic layers are the same and thus they differ only in the isotopic abundance of Fe. X-ray reflectivity data were fitted in order to get the total thickness of the films, which were used as normalization factors in order to determine the exact thicknesses of individual layers.

Figure 4 shows the SIMS depth profiles of ^{57}Fe, ^{54}Fe, ^{90}Zr, and ^{16}O in the as-deposited $Fe_{75}Zr_{25}$ isotopic marker layer film. ^{57}Fe shows a Gaussian peak at the marker layer position, whereas ^{54}Fe shows a dip at that position, so that the overall composition of the film remains constant. The

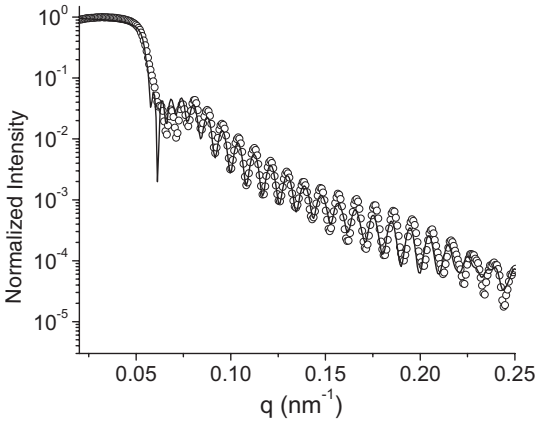

FIG. 3. X-ray reflectivity of the as-deposited amorphous $Fe_{75}Zr_{25}$ isotopic marker sample taken using Cu $K\alpha$ radiation.

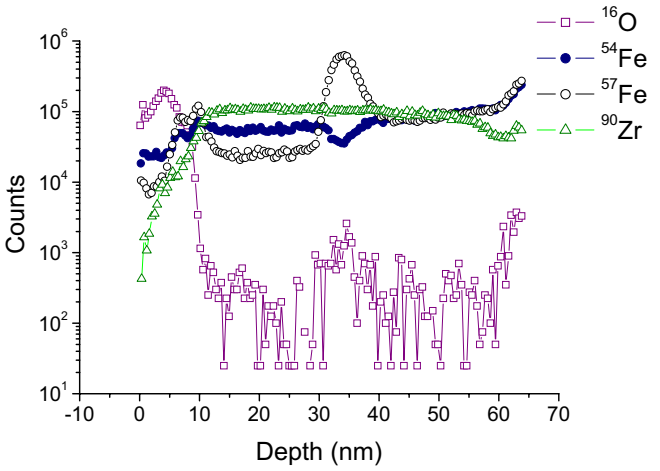

FIG. 4. (Color online) SIMS depth profile of various elements in as-deposited $Fe_{75}Zr_{25}$ marker sample.

oxygen content in the bulk of the film is negligibly small. ^{57}Fe enrichment in the marker layer comes out to be 40 at. %. A closer look at the depth profile of ^{57}Fe reveals that the peak is somewhat skewed toward higher sputtering time or larger depths. Such an asymmetry in the depth profile is due to radiation damage and small intermixing induced by the 4 keV Cs^+ ions used for sputtering the samples. A correction for this irradiation broadening of the profiles is applied to the primary concentration profiles. The concentration profiles are corrected to yield the true ones according to the following equation:[26,27]

$$C_r(x+h) = C_a(x) + h\frac{dC_a(x)}{dx}, \tag{1}$$

where $C_a(x)$ and $C_r(x)$ are the experimentally determined and true profiles, respectively, and h is a parameter that represents strength of intermixing due to Cs^+-ion bombardment. The value of h was determined by applying this correction on the as-deposited samples with known concentration profiles. The same value of h was used for correcting the depth profiles of the samples annealed at different temperatures. Figure 5 shows the depth profile of ^{57}Fe in as-deposited film, as obtained experimentally and after correction for irradiation broadening.

Figure 6 gives the x-ray diffraction (XRD) pattern of the marker layer film in pristine state as well as after annealing at different temperatures for 1 h each. The XRD pattern of the pristine film exhibits a broad hump in the angular range of 30°–50°, characteristic of an amorphous structure. The broad hump persists up to an annealing temperature of 673 K. Annealing at 773 K results in the appearance of an additional peak superimposed on the broad hump. The position of the additional peak corresponds to the (110) reflection of α-Fe. This shows that the amorphous structure is stable at least up to 673 K, while annealing at 773 K results in partial crystallization of the film, α-Fe being the primary phase precipitating out during crystallization. Furthermore, with thermal annealing, the shape of the amorphous hump exhibits significant variation, indicating structural relaxation. The

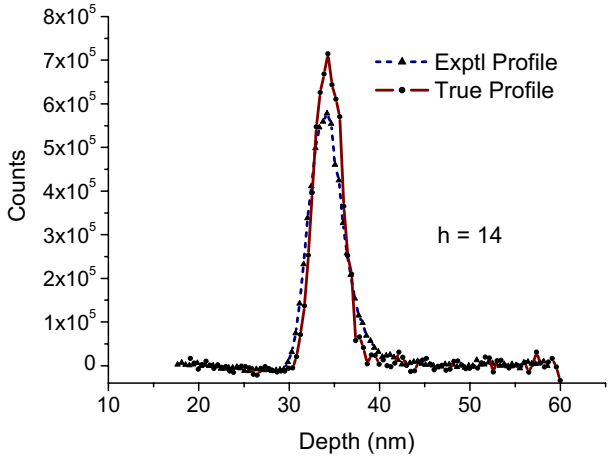

FIG. 5. (Color online) Depth profile of ^{57}Fe in as-deposited $Fe_{75}Zr_{25}$ marker sample, as obtained experimentally and after correcting for irradiation-induced intermixing.

broad hump is fitted with a Gaussian in order to yield the position and width of the same. The position of this peak is related with the average first-nearest-neighbor distance a through the relation[28] $a=1.23\lambda/2 \sin\theta$, where θ is the mean position of the broad maxima and λ is the wavelength of the x ray used ($\lambda=0.154$ nm). On the other hand, the width of the peak is a measure of the degree of disorder in the amorphous structure.

The variation in the average first-nearest-neighbor distance as well as the width of the amorphous hump as a function of thermal annealing temperature is shown in Fig. 7.

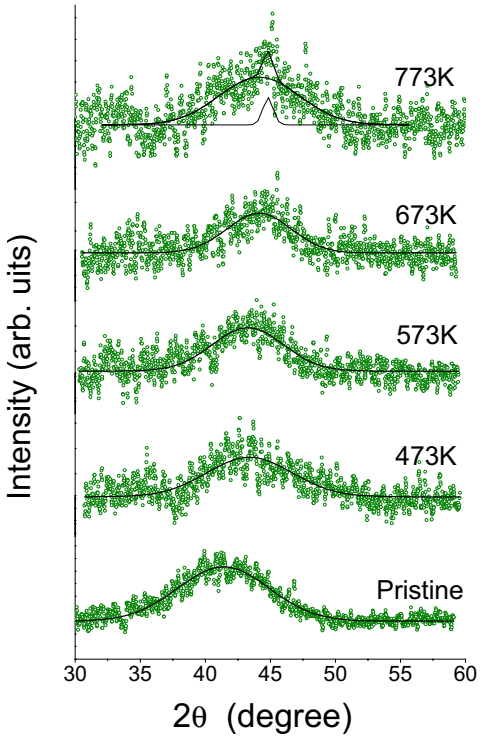

FIG. 6. (Color online) Grazing incidence x-ray-diffraction pattern of $Fe_{75}Zr_{25}$ film after annealing at different temperatures for 1 h each.

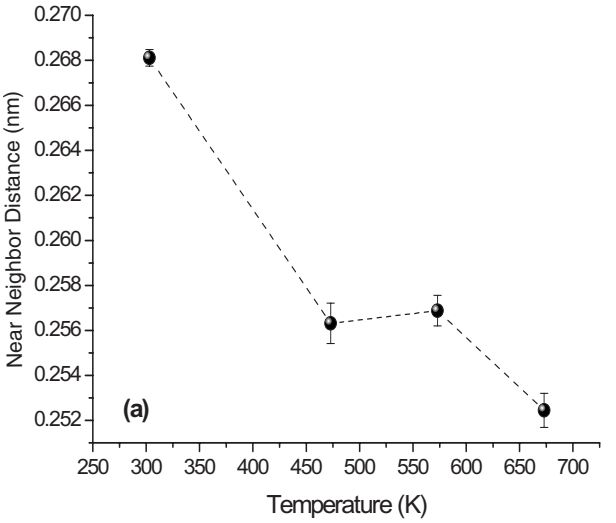

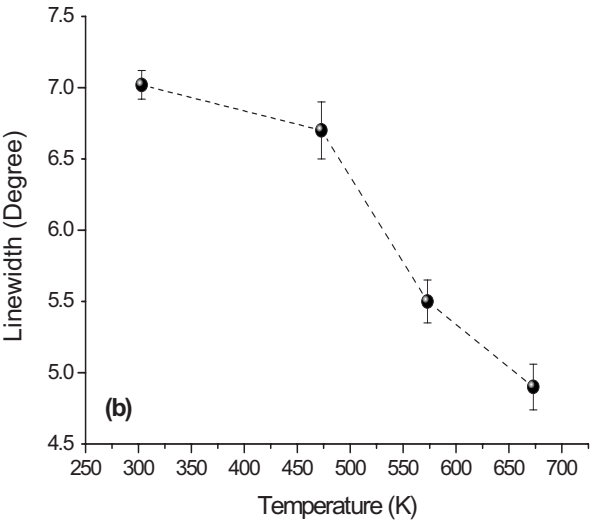

FIG. 7. Variations in (a) first-nearest-neighbor distance and (b) width of the amorphous hump, as functions of annealing temperature, as obtained from fitting of the XRD data.

Both these parameters exhibit significant variation with thermal annealing, indicating structural relaxation in the film. Structural relaxation in amorphous alloys is known to occur via two orthogonal atomic processes:[16,29] radial atomic motion results in changes in the density of the glass, while the short-range order of the glass is influenced by local atomic motion which conserves the density. The first process affects the average interatomic distance, while the second process affects the width of the diffraction maximum. The average nearest-neighbor distance is expected to decrease with thermal annealing as a result of the annihilation of the excess free-volume in the film. From Fig. 7(a) one may note that annealing at 473 K results in about 5% decrease in the nearest-neighbor distance. Further annealing up to 673 K results in only a small additional decrease. This suggests that most of the excess free volume in the film is annealed out after annealing at 473K for 1 h.

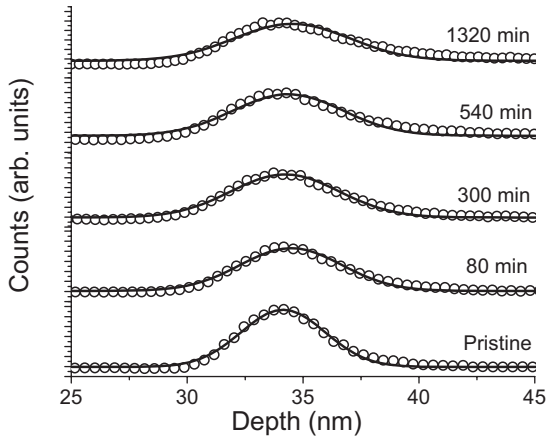

FIG. 8. SIMS depth profile of ^{57}Fe in as-deposited amorphous $Fe_{75}Zr_{25}$ marker sample as well as sample annealed isothermally at 563 K for different times. The scattered points (o) represent the experimental data and the solid line (—) represents the fitted Gaussian profiles.

From Fig. 7(b) one finds that the width of the amorphous hump shows only a small variation up to an annealing temperature of 473 K. Above 473 K the width exhibits a faster decrease. As the width of the amorphous hump is a measure of the degree of disorder and is related to the topological short-range order (TSRO) in the system,[16,29] a decrease in the width indicates an increase in the TSRO. Thus, up to 473 K, changes in the TSRO occur rather slowly, while beyond this temperature TSRO exhibits rapid improvement. The above results show that up to 473 K the structural relaxation mainly consists of the annihilation of the excess free volume, while above 473 K topological reordering dominates and continues at least up to 673 K.

B. Iron self-diffusion study using SIMS

Figure 8 gives typical SIMS depth profiles of the ^{57}Fe marker layer as a function of annealing time at 563 K. These profiles have been corrected for sputtering-induced intermixing at the interfaces using Eq. (1).

As the ^{57}Fe layer diffuses, its depth profile broadens and the diffusion length can be obtained using the relation

$$L_d^2 = \sigma_t^2 - \sigma_0^2, \tag{2}$$

where σ_t is the standard deviation of the ^{57}Fe depth profile after annealing for a time t. The diffusion length in turn is related to the diffusivity $D(T)$ at a given temperature T through the relation

$$L_d^2 = 2D(T)t. \tag{3}$$

Figure 9 gives the plot of the square of the diffusion length as a function of annealing time at three annealing temperatures, namely, 563, 623, and 653 K. One may note that initially L_d^2 increases rapidly with annealing time and gradually reaches a steady rate. Such a behavior of L_d^2 with annealing time is a result of structural relaxation in amorphous phase. In the presence of structural relaxation the instantaneous diffusivity can be written as[27,30]

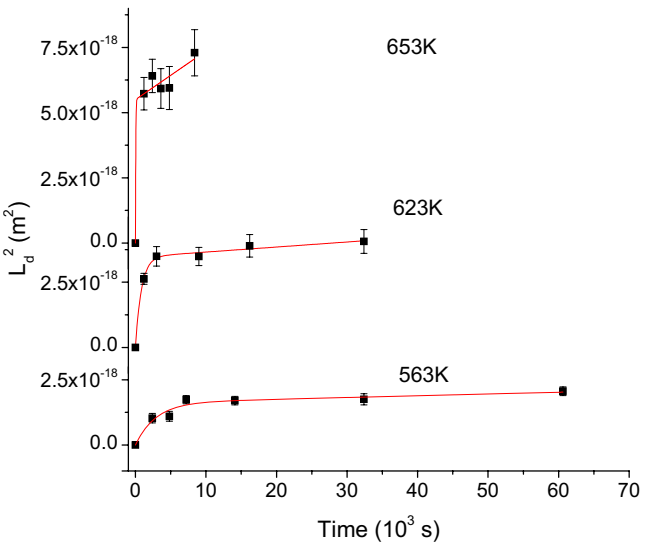

FIG. 9. (Color online) Annealing time dependence of the square of the diffusion length L_d^2 of iron in amorphous $Fe_{75}Zr_{30}$ isotopic marker layer film at various temperatures from SIMS measurements.

$$D(t) = A\ \exp(-t/\tau) + D_{SR}, \tag{4}$$

where D_{SR} is the diffusivity in the structurally relaxed state, τ is the relaxation time associated with the structural relaxation in the sample, and A is a quantity related to the diffusivity in the unrelaxed state. The average diffusivity $\langle D(t)\rangle = L_d^2(t)/2t$ is related to instantaneous diffusivity through the relation

$$\langle D(t)\rangle = \frac{L_d^2(t)}{2t} = \frac{1}{t}\int_0^t D(t')dt'. \tag{5}$$

Accordingly, the time dependence of $L_d^2(t)$ can be written as

$$L_d^2(t) = 2A\tau(1 - e^{-t/\tau}) + 2D_{SR}t. \tag{6}$$

The time dependence of L_d^2 in Fig. 9 is fitted with Eq. (6), in order to extract D_{SR}, τ, and A at each temperature. The diffusivity in the structurally relaxed state has been used to calculate the activation energy for diffusion using the relation

$$D_{SR} = D_0 \exp\left(-\frac{E}{k_B T}\right), \tag{7}$$

where E is the activation energy for diffusion and D_0 is the pre-exponential factor which is related to the mechanism of diffusion. In Fig. 10, the natural logarithm of diffusivity in the relaxed state is plotted as a function of the inverse of annealing temperature. Fit of this data with a straight line yields the value of activation energy $E=(1.2\pm0.3)$ eV and the pre-exponential factor $D_0=\exp(-29\pm5)$ m^2/s.

C. Iron self-diffusion study using nuclear-resonance reflectivity

At low temperatures diffusion length becomes small, making it necessary to do the measurements with higher accuracy as achievable using NRR. Therefore, diffusivity mea-

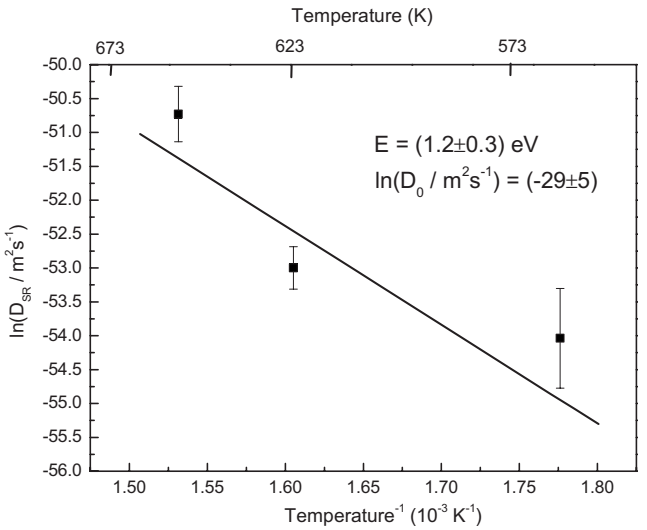

FIG. 10. Arrhenius plot for iron self-diffusion in structurally relaxed amorphous $Fe_{75}Zr_{25}$ isotopic marker layer sample.

surements at temperatures of 563 K and below were done using NRR on isotopic multilayer samples. Figure 11 gives the NRR of the isotopic multilayer annealed for different periods of time at 533 K. The intensity scale is multiplied by q^4, in order to remove the background due to Fresnel reflectivity.[31] In addition to the peak at critical angle for total reflection ($q=0.056$ nm^{-1}), the first Bragg peak due to isotopic periodicity is clearly visible. This is due to a strong scattering contrast between ^{57}Fe and ^{nat}Fe layers at the nuclear-resonance energy corresponding to the first excited state of ^{57}Fe nucleus (Mössbauer transition).[23,32,33]

With increasing annealing time, as the various isotopes of iron interdiffuse, the scattering contrast between the adjacent layers decreases, resulting in the decrease in the height of the Bragg peak. The diffusion length L_d is related to the change in the intensity of the Bragg peak through the relation[34,35]

$$\ln\left(\frac{I(t)}{I(0)}\right) = -\frac{4\pi^2 n^2}{\Lambda^2} L_d^2, \tag{8}$$

where Λ is the bilayer periodicity of the multilayer, n is the order of the Bragg peak, $I(0)$ is the height of the Bragg peak in as-deposited sample, and $I(t)$ is the height of the Bragg peak after annealing the sample for a time t at a particular temperature T. Figure 12 gives the plot of L_d^2 versus time for four different annealing temperatures, namely, 398, 473, 533, and 563 K, as obtained from NRR measurements. One may note that the diffusion length at 563 K, as obtained from SIMS measurement, is consistently higher than that obtained from NRR measurements. For example, after annealing for 8400 s, L_d from SIMS comes out to be 1.2 nm, while from NRR it comes out to be 0.9 nm. This difference may be due to possible minor differences in the preparation condition of the two samples (marker layer and multilayer), and due to different approximations involved in arriving at Eqs. (2) and (8). However, looking at the accuracy of measurements, particularly of SIMS, this difference is not very substantial. The data in Fig. 12 are fitted using Eq. (6) in order to extract D_{SR}, τ, and A. The diffusivity in the relaxed state D_{SR} at 398, 473, and 533 K comes out to be zero within the limits of experimental error. However, the relaxation time τ exhibits a systematic variation with annealing temperature (Fig. 13). The value of τ at 563 K as obtained from NRR measurements agrees with that obtained from SIMS measurement within experimental error. Since the variation in diffusivity with annealing time at a given temperature essentially occurs due to structural relaxation in the amorphous film, the relaxation time τ represents the time scale for structural relaxation.

IV. DISCUSSIONS

SIMS measurements provide the activation energy for diffusion of Fe in structurally relaxed state as $E=(1.2\pm0.3)$ eV and the corresponding pre-exponential factor $D_0=\exp(-29\pm5)$ m^2/s. It may be noted that a linear

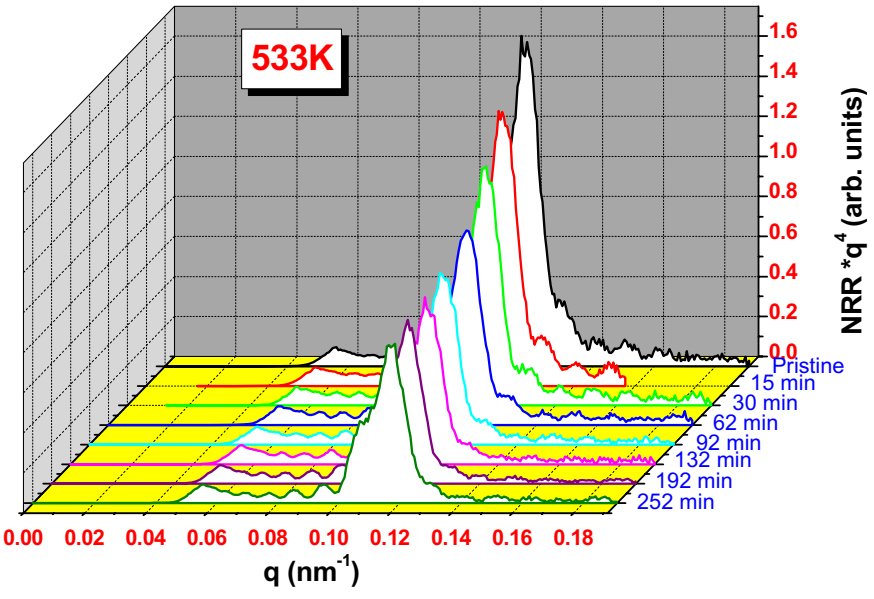

FIG. 11. (Color online) NRR ($^*q^4$) of $Fe_{75}Zr_{25}$ isotopic multilayer taken at the Mössbauer resonance energy of ^{57}Fe (14.413 keV), as a function of isothermal annealing at 533 K for different times. The Bragg peak around $q=0.11$ nm^{-1} corresponds to the isotopic periodicity of the multilayer.

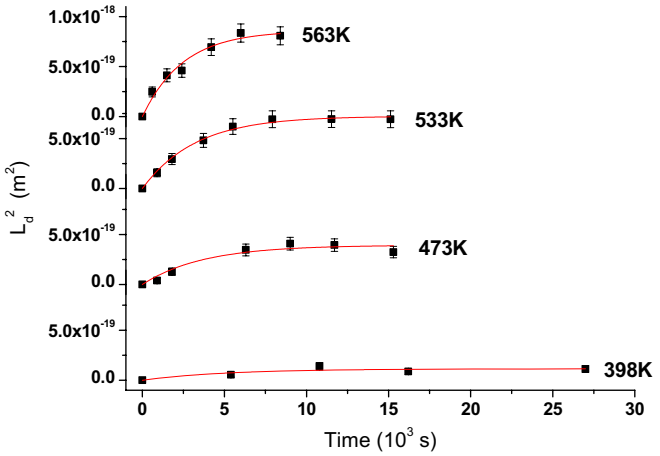

FIG. 12. (Color online) Annealing time dependence of the square of the diffusion length L_d^2 of iron in amorphous $Fe_{75}Zr_{30}$ isotopic multilayer film at various temperatures from NRR measurements.

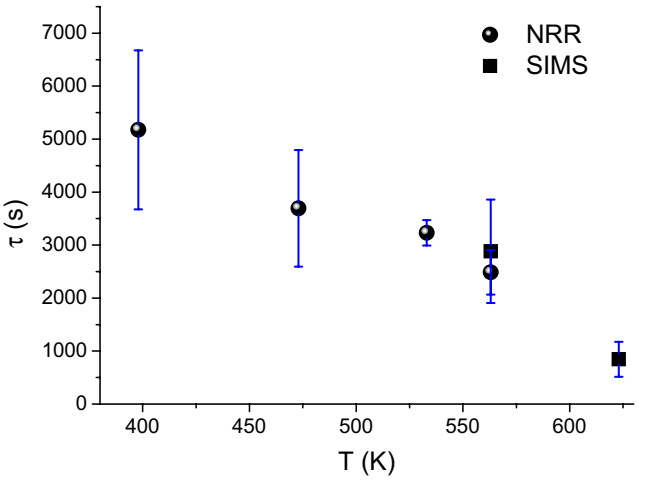

FIG. 13. (Color online) Plot of the relaxation time τ vs annealing temperature T. The results of both SIMS and NRR measurements are depicted.

correlation exists between $\ln D_0$ and E in the form[6,36,37]

$$\ln D_0 = \ln \alpha + E/\beta, \tag{9}$$

which holds for both amorphous and crystalline alloys. However, the values of α and β are very different in the two cases. In the case of amorphous alloys $\alpha = 10^{-19}$ m^2/s and $\beta = 0.055$ eV and for crystalline alloys $\alpha = 10^{-7}$ m^2/s and $\beta = 0.41$ eV.[6] Figure 14 gives the plot of $\ln D_0$ vs E for various amorphous and crystalline alloys. The dotted line shows the correlation of $\ln D_0$ with E for amorphous alloys. The values obtained for the $Fe_{75}Zr_{25}$ alloy in the present case agree very well with this correlation. Following Shewmon[38] the pre-exponential factor D_0 can be expressed as[6]

$$\ln D_0 = \ln(ga^2 f \upsilon_0) + \left(\frac{\Delta S}{k_B}\right), \tag{10}$$

where g is a geometric factor, a is the effective jump distance, υ_0 is the effective jump frequency, f is the correlation factor, and ΔS is the entropy of diffusion. Comparing Eqs. (9) and (10) one finds

$$\alpha = ga^2 f \upsilon_0 \quad \text{and} \quad \beta = k_B E/\Delta S. \tag{11}$$

Taking the known value of β for amorphous alloys, the value of entropy for diffusion in the present case comes out to be about $22k_B$. This large value of ΔS as compared to that in the case of crystalline alloys reflects a different mechanism of diffusion in amorphous alloys, which involves collective jumps of a large group of atoms.[6,39]

From Eq. (4), the diffusivity at $t=0$, i.e., in the unrelaxed state, is given by

$$D(0) = A + D_{SR}. \tag{12}$$

Figure 15 depicts the variation in $\ln[D(0)]$ versus 1/T for all the temperatures covering both SIMS and NRR measurements. One can discern two distinct temperature regimes: the data in the temperature range of 533–623 K can be fitted with a straight line, yielding the activation energy for diffusion as (1.0 ± 0.1) eV. At lower temperatures, $\ln[D(0)]$ exhibits a systematic deviation from this curve, yielding a lower activation energy of (0.32 ± 0.05) eV. It is interesting to note that in the temperature regime of 533–653 K, the activation energy for diffusion in the unrelaxed state comes out to be the same as that in the fully relaxed state, while in the lower-temperature regime the activation energy in the unrelaxed state is substantially lower than that in the relaxed state. From Fig. 7(a) one finds that thermal annealing at 473 K for 1 h results in almost complete annihilation of the excess free volume. Therefore, in the higher-temperature regime (533–653 K) which is well above 473 K, excess free volume is expected to get annihilated in a short time. Thus, the observed time dependence of diffusivity in this temperature range arises mainly due to time-dependent relaxation of topological short-range order. As a result, the extrapolated value of $D(0)$, as obtained from the time dependence of average diffusivity using Eq. (6), pertains to a partially relaxed state in which topological relaxation has not yet occurred, while excess free volume is largely annihilated out. On the other hand, in the lower-temperature regime, the time dependence of diffusivity mainly arises due to annihilation of excess free volume (as the topological structural relaxation occurs at a very slow rate in this temperature range). Therefore, the extrapolated value of $D(0)$ pertains to the truly unrelaxed state, in which neither the relaxation of topological short-range order nor the annihilation of excess free volume has taken place. The fact that in the higher-temperature regime the activation energy for $D(0)$ is comparable to that in the relaxed state suggests that it is mainly the presence of excess free volume that results in the lowering of the activation energy for diffusion in the unrelaxed state.

As discussed earlier, the correlation of the activation energy with $\ln(D_0)$ provides information about the mechanism of diffusion in the system. The data points corresponding to the two regimes of diffusivity in the unrelaxed state are also plotted in Fig. 14. One may note that both points lie along the correlation line corresponding to the amorphous alloys. This suggests that, even in the unrelaxed state, the mechanism of diffusivity remains the same; i.e., it involves a col-

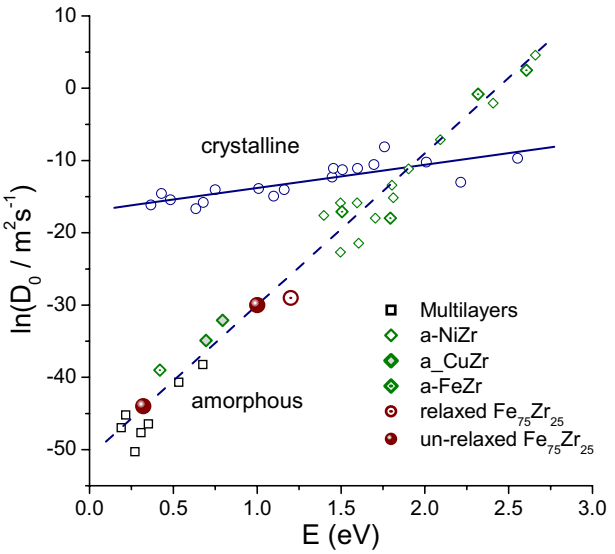

FIG. 14. (Color online) Plot of $\ln D_0$ vs E for various amorphous and crystalline alloys showing correlation between the two quantities. Amorphous and crystalline systems exhibit distinctly different $\ln D_0 - E$ correlations. Data points for amorphous $Fe_{70}Zr_{30}$ in both relaxed and unrelaxed states, as obtained in the present work, are also plotted.

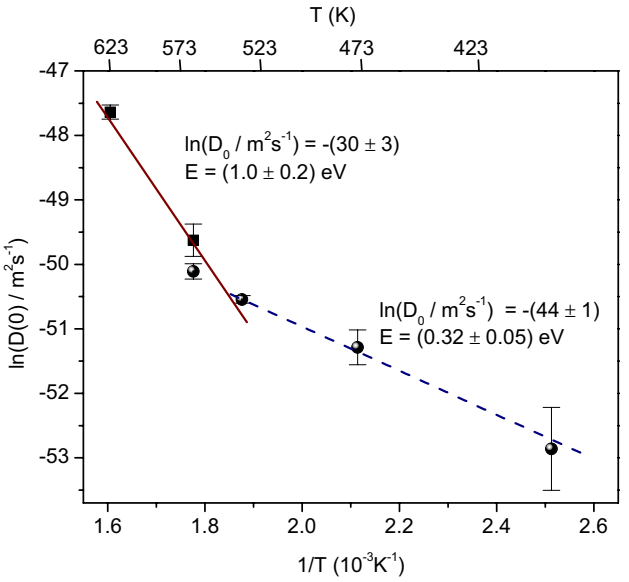

FIG. 15. (Color online) Arrhenius plot for iron self-diffusion in unrelaxed amorphous $Fe_{75}Zr_{25}$. Results of both SIMS and NRR measurements are depicted.

lective jump of a group of atoms, although the diffusivity in the unrelaxed state is substantially higher than in the relaxed state. Using Eq. (11), the entropies for diffusion ΔS in the two regimes of diffusivity in the unrelaxed state come out to be $20k_B$ (higher-temperature regime) and $6k_B$ (lower-temperature regime). In some recent studies,[40,41] a possible difference in the mechanism of diffusion in unrelaxed and relaxed states of amorphous CoZr alloy films has been studied through the isotope effect, defined as

$$IE = \frac{D_i/D_j - 1}{\sqrt{(m_j/m_i)} - 1}, \tag{13}$$

where D_i (D_j) and m_i (m_j) are the diffusivity and mass of the isotope i (j), respectively. It has been found that the isotope effect remains negligible in both relaxed and unrelaxed states. Small IE values were interpreted as resulting from a strong dilution of the mass effect through participation of a group of atoms in the diffusion process. In contrast to this, measurements of self-diffusion in densely packed crystalline metals result in a high isotope effect of $IE \approx 0.7$,[42] and are interpreted as single-atom jumps via vacancies. In molecular-dynamics simulation of atomic diffusion in $Fe_{91}Zr_9$, it is found that an artificial introduction of vacancies in a relaxed glass structure results in higher self-diffusivities. However, these vacancies are dynamically unstable and dissolve after a few jumps.[43] These studies again support a collective mechanism for atomic diffusion in amorphous alloys. The present results, while in agreement with these earlier findings,[40,41,43] provide a deeper insight into the mechanism of diffusion in the unrelaxed state: we find that although the mechanism of diffusion involves a collective jump of a group of atoms in both unrelaxed and relaxed amorphous states, the average number of atoms participating in a diffusive jump exhibits variation in different regimes. In the lower-temperature range, where the quenched-in excess free volume is still not annihilated out, the average number of atoms participating in a diffusive jump is only 6, as compared to 22 in the relaxed state. Thus, the present results show that the presence of excess free volume in unrelaxed amorphous films results in significant modification in the atomic-level processes involved in diffusion: (i) activation energy for diffusion is substantially reduced, and (ii) diffusive jumps are less cooperative in nature, involving a smaller number of atoms. These results can be understood in terms of the free-volume model developed for liquids and also applied extensively to metallic glasses and polymers,[44–47] according to which the diffusivity can be written as

$$D = D_0 \exp\left(-\frac{\gamma v^*}{v_f}\right), \tag{14}$$

where v^* is the critical volume of a void, created as a result of random redistribution of free volume, sufficiently large for an atom to move in, v_f is the mean free volume per atom, and γ is an overlap factor with value between 0.5 and 1. The temperature dependence of v_f, e.g., due to thermal expansion, leads to temperature dependence of diffusivity. The presence of an excess free volume in the unrelaxed state would result in an increase in v_f, thus resulting in a decrease in the activation energy. Further, the viscosity η of metallic glasses is known to increase with the annihilation of excess free volume.[46] A higher viscosity means a more cooperative motion of atoms and involvement of a larger group of atoms in a diffusive jump. This would lead to an increase in ΔS when the excess free volume is annealed out due to structural relaxation.

These results are significant in the context of amorphous thin films since physical vapor-deposition technique, which is generally used for depositing amorphous films, has a much

higher effective quenching rate as compared to amorphous ribbons produced by melt spinning. This would result in a higher quenched-in free volume, thus modifying the diffusion behavior.

In Sec. III A it was seen that annealing at 473 K for 1 h results in annihilation of most of the excess free volume. From Fig. 12 one finds that the diffusion length achieved after such an annealing treatment is ~0.7 nm. This is also consistent with the length scale of the structural fluctuations seen by neutron small-angle scattering in metallic glasses[48] and also in x-ray scattering.[16]

V. CONCLUSION

In conclusion, self-diffusion of Fe in amorphous $Fe_{75}Zr_{25}$ alloy has been studied over a wide temperature range from 398 to 653 K by combining the results of SIMS and NRR measurements. The high accuracy with which diffusion length can be measured using NRR allows one to follow quantitatively the diffusivity during structural relaxation. A distinct correlation of diffusivity with various types of structural relaxations in the system has been observed. In the fully relaxed state the activation energy for diffusion comes out to be (1.2 ± 0.3) eV. The observed value of the pre-exponential factor D_0 suggests that similar to other amorphous alloys, diffusion jumps in this system involve a large group of atoms. It is found that, even in unrelaxed or partially relaxed states, the diffusion mechanism involves collective motion of a group of atoms and not a vacancy-mediated jump. However, the presence of excess free volume results in a decrease in the number of the atoms participating in a diffusive jump, and also in a decrease in the activation energy. The present study shows that the typical diffusion length involved in annihilation of excess free volume is ~0.7 nm. This length scale is consistent with that of structural fluctuations seen by neutron small-angle scattering.

ACKNOWLEDGMENT

Financial support from the Indo-French Center for Propmotion of Advanced Research is acknowledged.

*agupta@csr.ernet.in

†Present address: Technische Universität Clausthal, Institut für Metallurgie, D-38678 Clausthal-Zellerfeld, Germany.

[1] H. Kubota, A. Fukushima, K. Yakushiji, T. Nagahama, S. Yuasa, K. Ando, H. Maehara, Y. Nagamine, K. Tsunekawa, D. D. Djayaprawira, N. Watanabe, and Y. Suzuki, Nat. Phys. **4**, 37 (2008); J. Scola, H. Polovy, C. Fermon, M. Pannetier-Lecoeur, G. Feng, K. Fahy, and J. M. D. Coey, Appl. Phys. Lett. **90**, 252501 (2007).

[2] J. Y. Bae, W. C. Lim, H. J. Kim, T. D. Lee, K. W. Kim, and T. W. Kim, J. Appl. Phys. **99**, 08T316 (2006).

[3] Y. Luo, M. Esseling, A. Käufler, K. Samwer, T. Dimopoulos, G. Gieres, M. Vieth, M. Rührig, J. Wecker, C. Rudolf, T. Niermann, and M. Seibt, Phys. Rev. B **72**, 014426 (2005); J. Hayakawa, S. Ikeda, F. Matsukura, H. Takahashi, and H. Ohno, Jpn. J. Appl. Phys., Part 2 **44**, L587 (2005).

[4] J. J. Yang, Ying Yang, Kaisheng Wu, and Y. Austin Chang, J. Appl. Phys. **98**, 074508 (2005); A. Pérez-Junquera, G. Rodríguez-Rodríguez, M. Vélez, J. I. Martín, H. Rubio, and J. M. Alameda, *ibid.* **99**, 033902 (2006).

[5] Kazuo Shimamura, Yoshiaki Matsumoto, and Tsunebumi Matsunaga, Surf. Coat. Technol. **50**, 127 (1992); Ryuichi Tarumi, Akira Shibata, Hirotsugu Ogi, Masahiko Hirao, Kazuki Takashima, and Yakichi Higo, J. Appl. Phys. **101**, 053519 (2007); K. Takashima, Y. Higo, S. Sugiura, and M. Shimojo, Mater. Trans. **42**, 68 (2001).

[6] F. Faupel, W. Frank, M.-P. Macht, H. Mehrer, V. Naundorf, K. Rätzke, H. R. Schober, S. K. Sharma, and H. Teichler, Rev. Mod. Phys. **75**, 237 (2003).

[7] W. Frank, Defect Diffus. Forum **143-147**, 695 (1997).

[8] W. Frank, A. Hörner, P. Scharwaechter, and H. Kronmüller, Mater. Sci. Eng., A **179-180**, 36 (1994).

[9] Mukul Gupta, Ajay Gupta, S. Rajagopalan, and A. K. Tyagi, Phys. Rev. B **65**, 214204 (2002).

[10] Mukul Gupta, Ajay Gupta, S. Chakravarty, R. Gupta, and T. Gutberlet, Phys. Rev. B **74**, 104203 (2006).

[11] S. G. Mayr, J. Appl. Phys. **97**, 096103 (2005).

[12] V. H. Hammond, M. D. Houtz, and J. M. O'Reilly, J. Non-Cryst. Solids **325**, 179 (2003).

[13] T. Egami, IEEE Trans. Magn. **17**, 2600 (1981); H. S. Chen, J. Appl. Phys. **49**, 3289 (1978).

[14] M. R. J. Gibbs and G. Hygate, J. Phys. F: Met. Phys. **16**, 809 (1986); H. S. Chen, Solid State Commun. **33**, 915 (1980).

[15] J. O. Ström-Olsen, R. Brüning, Z. Altounian, and D. H. Ryan, J. Less-Common Met. **145**, 327 (1988); H. S. Chen, R. C. Sherwood, H. J. Leamy, and E. M. Gyorgy, IEEE Trans. Magn. **12**, 933 (1976); H. H. Liebermann, C. D. Graham, and P. J. Flanders, *ibid.* **13**, 1541 (1977).

[16] R. Brüning and J. O. Ström-Olsen, Phys. Rev. B **41**, 2678 (1990).

[17] W. Dmowski, C. Fan, M. L. Morrison, P. K. Liaw, and T. Egami, Mater. Sci. Eng., A **471**, 125 (2007).

[18] Ajay Gupta, M. E. Jayaraj, and S. Habibi, Phys. Rev. B **48**, 274 (1993).

[19] B. Cantor and R. W. Cahn, in *Amorphous Metallic Alloys*, edited by F. E. Luborsky (Butterworth, London, 1983), p. 487.

[20] Ajay Gupta, Dileep Kumar, and Carlo Meneghini, Phys. Rev. B **75**, 064424 (2007).

[21] J. Lu, P. L. Kuhns, M. J. R. Hoch, W. G. Moulton, and A. P. Reyes, Phys. Rev. B **72**, 054401 (2005).

[22] V. M. Uzdin and L. Häggström, Phys. Rev. B **72**, 024407 (2005).

[23] Ajay Gupta, Mukul Gupta, Sujoy Chakravarty, Rudolf Rüffer, Hans-Christian Wille, and Olaf Leupold, Phys. Rev. B **72**, 014207 (2005).

[24] Mukul Gupta, Ajay Gupta, D. M. Phase, S. M. Chaudhari, and B. A. Dassanacharya, Appl. Surf. Sci. **205**, 309 (2003).

[25] R. Rüffer and A. I. Chumakov, Hyperfine Interact. **97-98**, 589

(1996); See also, http://www.esrf.eu/UsersAndScience/Experiments/HRRS/NRG
[26] G. Brebec, R. Seguin, C. Sella, J. Bevenot, and J. C. Martin, Acta Metall. **28**, 327 (1980).
[27] Y. Loirat, J. L. Boequet, and Y. Limoge, J. Non-Cryst. Solids **265**, 252 (2000).
[28] A. Guinier, *X-Ray Diffraction in Crystals, Imperfect Crystals, and Amorphous Bodies* (Dover, New York, 1994).
[29] M. Mao, Z. Altounian, and R. Bruning, Phys. Rev. B **51**, 2798 (1995).
[30] A. K. Tyagi, M.-P. Macht, and V. Naundorf, Acta Metall. Mater. **39**, 609 (1991).
[31] L. G. Parratt, Phys. Rev. **95**, 359 (1954).
[32] Ajay Gupta, Mukul Gupta, B. A. Dasannacharya, Y. Yoda, S. Kikuta, and M. Seto, J. Phys. Soc. Jpn. **73**, 423 (2004).
[33] A. I. Chumakov, G. V. Smirnov, A. Q. R. Baron, J. Arthur, D. E. Brown, S. L. Ruby, G. S. Brown, and N. N. Salashchenko, Phys. Rev. Lett. **71**, 2489 (1993).
[34] T. Mizoguchi, S. Tanabe, and M. Murata, J. Magn. Magn. Mater. **126**, 96 (1993).
[35] A. L. Greer and F. Spaepen, in *Synthetic Modulated Structures*, edited by L. L. Chang and B. C. Giessen (Academic, Orlando, 1985), p. 419.
[36] W. Linert, Chem. Soc. Rev. **18**, 477 (1989).
[37] Wei-Hua Wang, Hai Yang Bai, Ming Zhang, J. H. Zhao, X. Y. Zhang, and W. K. Wang, Phys. Rev. B **59**, 10811 (1999).
[38] P. G. Shewmon, *Diffusion in Solids* (Minerals, Metals, and Materials Society, Warrendale, PA, 1989).
[39] S. K. Sharma and F. Faupel, J. Mater. Res. **14**, 3200 (1999).
[40] A. Heesemann, K. Rätzke, V. Zöllmer, and F. Faupel, New J. Phys. **3**, 6 (2001).
[41] V. Zöllmer, H. Ehmler, K. Rätzke, P. Troche, and F. Faupel, Europhys. Lett. **51**, 75 (2000).
[42] P. W. Hüppe and F. Faupel, Phys. Rev. B **46**, 120 (1992).
[43] W. Frank, U. Hamlescher, H. Kronmüller, P. Scharwaechter, and T. Schuler, Phys. Scr. **T66**, 201 (1996).
[44] M. H. Cohen and D. Turnbull, J. Chem. Phys. **31**, 1164 (1959).
[45] M. H. Cohen and G. S. Grest, J. Non-Cryst. Solids **61-62**, 749 (1984).
[46] F. Spaepen, Mater. Sci. Eng. **97**, 403 (1988).
[47] F. Faupel and K. Rätzke, in *Diffusion in Condensed Matter, Methods, Materials, Models*, edited by P. Heitjans and J. Kärger (Springer, Berlin, 2005), p. 250.
[48] P. Lamparter and S. Steeb, J. Non-Cryst. Solids **106**, 137 (1988).